Available online at www.sciencedirect.com
ScienceDirect
Trans. Nonferrous Met. Soc. China 23(2013) 2147−2152
Transactions of Nonferrous Metals Society of China
www.tnmsc.cn

Surface energies and appearances of commonly exposed surfaces of scheelite crystal

Zhi-yong GAO, Wei SUN, Yue-hua HU, Xiao-wen LIU

School of Minerals Processing and Bioengineering, Central South University, Changsha 410083, China

Received 7 June 2012; accepted 28 September 2012

Abstract: Surface energies of five different surfaces of scheelite crystal were calculated using density functional theory (DFT). Based on the calculation results, the predominantly exposed surfaces in the morphologies of scheelite crystals were predicted. {112} and {001} cleavage surfaces and {112} crystal surface are the commonly exposed surfaces, which are consistent with both previous literatures and the present experimental observations based on the XRD. Cleavage generates more easily along {112} surfaces than along {001} surfaces due to their different interlayer spacings. The surface roughness and appearance of different predominantly exposed surfaces were then investigated using AFM. The roughness of smooth {112} cleavage surface is the lowest among these three surfaces. On {001} cleavage surface, terraces are flat and separated by steps of about 10 nm in height. Subsequently, contact angle measurements were adopted to evaluate the wettability and surface energies of these surfaces. The surface energies evaluated directly correspond to the trend calculated with DFT.

Key words: scheelite; surface energy; cleavage; contact angle; wettability

1 Introduction

As an important ore mineral of tungsten, scheelite $CaWO_4$ is commonly associated with other calcium-bearing minerals in mineral ore deposits, such as calcite $CaCO_3$, apatite $Ca_{10}(PO_4)_6F_2$ and fluorite CaF_2 [1]. With the increasing need of low-grade complex ores processing, more scheelite is to be separated by means of flotation from these calcium-bearing minerals. Since flotation, as a surface-chemistry based process for separation of fine ores, takes advantage of the different wettability on mineral particle surfaces, the understanding of surface structures and properties of commonly exposed scheelite surfaces becomes important. To our knowledge, however, few theoretical and experimental studies were conducted on scheelite surfaces. Only recently, the interaction of water and a selection of small organic surfactant molecules (i.e. methanoic acid, hydroxyl methanamide, methylamine and hydroxyl ethanol) on different surfaces of scheelite [2,3] were investigated with the computer simulations. In addition, five families of slip systems and anisotropic microhardness and fracture in natural single scheelite crystal were studied using TEM and interpreted by means of anisotropic crystallographic structure of scheelite [4,5]. The recent study on calcite and fluorite crystals showed that the dangling bond density and wettability of these two crystals exhibited anisotropy [6].

In this study, surface energies of five different surfaces of scheelite crystal were calculated using density functional theory (DFT). The predominant cleavage surfaces and preferential expressed crystal surfaces of scheelite were predicted according to the calculation results, which were then compared with the observations based on XRD. These commonly exposed surfaces were carefully selected from natural scheelite crystal samples to study their roughness and appearance by AFM. Contact angle measurements were used to evaluate the wettability and surface energies of these commonly exposed surfaces.

2 Experimental

2.1 Surface energy calculation

The thermodynamic stability of a given surface is

Foundation item: Project (50831006) supported by the National Natural Science Foundation of China; Project (CX2011B122) supported by Hunan Provincial Innovation Foundation for Postgraduate, China; Project (2012BAB10B05) supported by the National Key Technologies R&D Program of China

Corresponding author: Yue-hua HU; Tel: +86-731-88879299; E-mail: HYH@ csu.edu.cn

DOI: 10.1016/S1003-6326(13)62710-7

dependent on its surface energy. A low and positive value indicates a stable surface, which is important in the morphology of the mineral. The surface energy (E_{surf}) in a slab model [7] could be calculated by

$$E_{surf}=[E_{slab}-(N_{slab}/N_{bulk})E_{bulk}]/(2A) \quad (1)$$

where E_{slab} and E_{bulk} are the total energies of the surface slab and the bulk unit cell, respectively; N_{slab} and N_{bulk} are the numbers of atoms contained in the slab and the bulk unit cells, respectively; A is the unit area of the surface; 2 denotes two surfaces along the z-axis in the surface slab.

The surface energy was calculated using the CASTEP module in Material Studio 5.0 on the basis of density function theory (DFT) [8]. The exchange-correlation energy was described by generalized gradient approximation of Perdew–Burke–Ernzerhof (GGA-PBE) [9]. The completeness of the basis set was determined by a kinetic energy cutoff, E_{cut}. All calculations were performed using a cutoff energy of 340 eV. Reciprocal space integration over the Brillouin zone was approximated with finite sampling of k-point using the Monkhorst–Pack scheme, and the k-point spacing was set to be 0.04 $Å^{-1}$. The structures were relaxed using a Broyden−Fletcher−Goldfarb−Shanno (BFGS) scheme, with the following thresholds for the converged structure: energy change per atom was less than 1.0×10^{-5} eV, residual force was less than 0.03 eV/Å, the displacement of atoms during the geometry optimization was less than 0.001 Å, and the residual bulk stress was less than 0.05 GPa.

The crystal structure of scheelite was built in crystal builder module using the structure data from KAY et al [10], and optimized according to GGA-PBE. A range of surface slabs was then created from the optimized bulk unit cell of scheelite at its Miller indices by surface builder module in materials studio (MS). Taking {001} surface cells as example, the convergence tests of the surface energy with respect to slab depths were conducted, and the results are illustrated in Table 1. Three more layers within the slab were found to be adequate to converge the surface energies within 0.001 J/m^2. In this study, a slab which has the thickness of 3 atomistic layers perpendicular to the surface and could be infinitely extended in the other two directions, was used to simulate the scheelite surface in periodic boundary conditions. Surface cells were separated from repeated replicas by a certain vacuum width of 12 Å. The different surface cells used for surface energy calculation are shown in Fig. 1. The calculated surface energies of five scheelite surfaces are listed in Table 1.

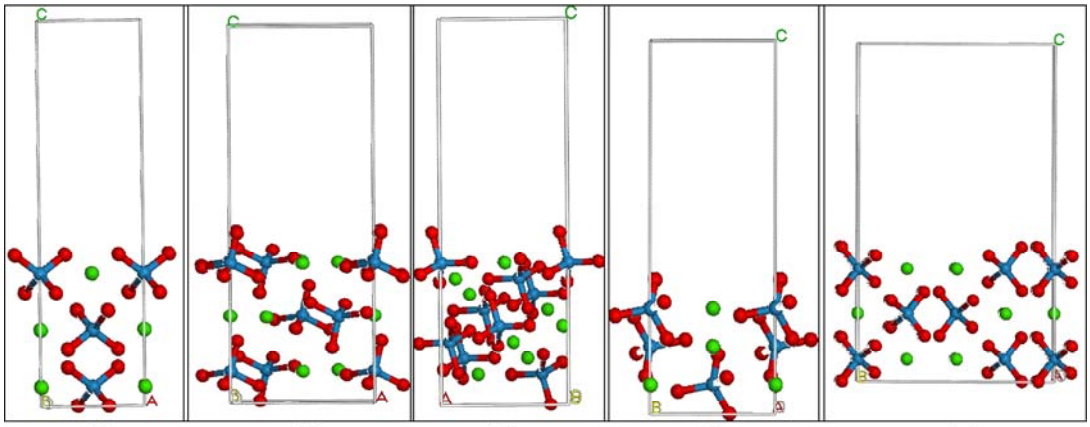

Fig. 1 Side views of crystal structures of different surface cells of scheelite crystal used for surface energy calculation: (a) {001)}; (b) {112}; (c) {111}; (d) {110}; (e) {100} (●—Ca; ●—O; ●—W)

Table 1 Total energies of surface cells and surface energies of different surfaces of scheelite

Crystal surface	a/Å	b/Å	c/Å	Atomistic layers within surface slab	Total energy/eV	Cell formula	Surface energy/ ($J\cdot m^{-2}$)
{001}	5.3267	5.3267	13.9660	1	−4688.3468	$CaWO_4$	0.4279
	5.3267	5.3267	16.8587	2	−9378.3426	$Ca_2W_2O_8$	0.3904
	5.3267	5.3267	19.7515	3	−14068.0937	$Ca_3W_3O_{12}$	0.4218
	5.3267	5.3267	22.6442	4	−18757.9550	$Ca_4W_4O_{16}$	0.4222
	5.3267	5.3267	25.5370	5	−23447.8198	$Ca_5W_5O_{20}$	0.4216
{112}	7.5331	6.9035	21.8503	3	−28135.9690	$Ca_6W_6O_{24}$	0.4939
{111}	7.5331	12.7382	21.6727	8	−37512.5075	$Ca_8W_8O_{32}$	0.5337
{110}	6.9035	6.9035	18.7074	3	−14060.2764	$Ca_3W_3O_{12}$	0.6086
{100}	5.3267	11.5710	19.9027	3	−28132.8362	$Ca_6W_6O_{24}$	0.8239

Note: The total energy of a unit cell with formula $Ca_2W_2O_8$ of scheelite crystal is −9379.7253 eV.

2.2 Materials

Natural single crystal scheelite from the Xianghuapu Mine was supplied by JWFU® (Shanghai, China) and used for contact angle measurements. The commonly exposed cleavage and crystal surfaces were carefully selected or cleaved to avoid cracks and inclusions. The crystallographic orientation of the specimen was determined by single-crystal X-ray diffraction. After cleaving, the samples were cleaned with a puff of 99.999% pure nitrogen gas to mechanically remove the scheelite dust produced during preparation. Deionized water from atomic adsorption-type ultrapure water system (resistivity 18 MΩ·cm), formamide (99%, Adamas), and diiodomethane (99%, Adamas) were employed as probe liquids for contact angle measurements.

2.3 XRD

X-ray diffractometer (D8-ADVANCE Bruker-AXS) was run in the reflection mode with Cu K_α radiation (λ=1.5406, tube potential 40 mV, tube current 40 mA), and a goniometer speed of 4 (°)/min. The single-crystal diffraction patterns with a 0.01° precision of interlayer spacing (d) measurements were conducted from 5° to 80° (2θ).

2.4 AFM imaging

Nanoscope Multimode IIIa AFM (Digital Instruments, CA) with software version 7.30r1 was used for capturing and analyzing images of scheelite surfaces. All AFM experiments were carried out in tapping mode in air at room temperature (20±2) °C. Scan area was set to be 2 μm×2 μm so that images could be compared more easily. Scan rate was kept constant at 1.0 Hz to obtain stable images.

2.5 Contact angle measurements

Static contact angles of the probe liquids on the sample surfaces were measured using GBX contact angle meter (France) equipped with a digital camera and computer software for the contact angle calculation from the shape of the settled droplet. A liquid drop of about 3.5 μL was placed on the sample surface, and the readings of contact angles were taken automatically on the left and right sides of the water droplet profile by computer software. Measurements of the contact angles were conducted at room temperature of 20 °C. At least 3 contact angle measurements were taken for each probe liquid on each sample surface.

3 Results and discussion

3.1 Validation of simulation methods

Scheelite has a tetragonal crystal structure with a=b=5.243 Å, c=11.376 Å, and α=β=γ=90° [10,11]. To establish the validity of the GGA-PBE for modeling scheelite surfaces, the scheelite crystal structure was optimized and compared with the experimentally observed values. Upon geometry optimization with GGA-PBE, the lattice parameters of scheelite crystal are a=b=5.327 Å, c=11.571 Å, and α=β=γ=90°, which are in reasonable agreement with those reported experimentally.

3.2 Surface energies and cleavage properties of scheelite crystal

The equilibrium morphology of a crystal is determined by its surface energy and the related growth rate of various surfaces [2]. More specifically, a surface with a high surface energy was expected to have a large growth rate and this fast growing surface would not be expressed in the resulting crystal morphology. Surfaces with low surface energies and hence slow growing rates would be expressed only. The thermodynamic penalty for cleaving a surface from a bulk material was also measured according to the surface energy. The calculated surface energies of all five surfaces are shown in Table 1. According to Table 1, surface energies of different scheelite surfaces followed the order of {100}>{110}>{111}>{112}>{001}. {001} and {112} surfaces with the lowest surface energies were the dominant cleavage and/or expressed planes in the equilibrium morphology of scheelite crystal. It was encouraging to note that this prediction agreed well with the previous literatures [4,5,12,13] and the present experimental observations based on XRD. The XRD results, as shown in Fig. 2, revealed a large degree of {112} and {001} preferred orientation in morphological measurements of a set of about 20 crystal specimens, possibly indicating preferred cleavage on these two surfaces and the natural tendency to preferential {112} growth for scheelite crystal.

It was worth mentioning that all Ca atoms had two broken (dangling) bonds while O atoms had one broken bond on {112} and {001} surfaces. Their different surface energies might attribute to the density of surface broken bonds obtained in the way that the number of broken (dangling) bonds divided by unit area on each surface. The calculated surface broken bond density was about 0.1455 $Å^{-2}$ for {001} surface and 0.1588 $Å^{-2}$ for {112} surface. A larger surface broken bond density of {112} surface led to a more reactive and unstable surface, hence a higher surface energy. In addition, the cleavage generated much easily along {112} surfaces than along {001} surfaces due to their different interlayer spacings. COOPER and de LEEUW [3] held that when the mineral particles were crushed in the first stage of flotation process, the minerals would mainly cleave along surfaces that had large interlayer spacings. The

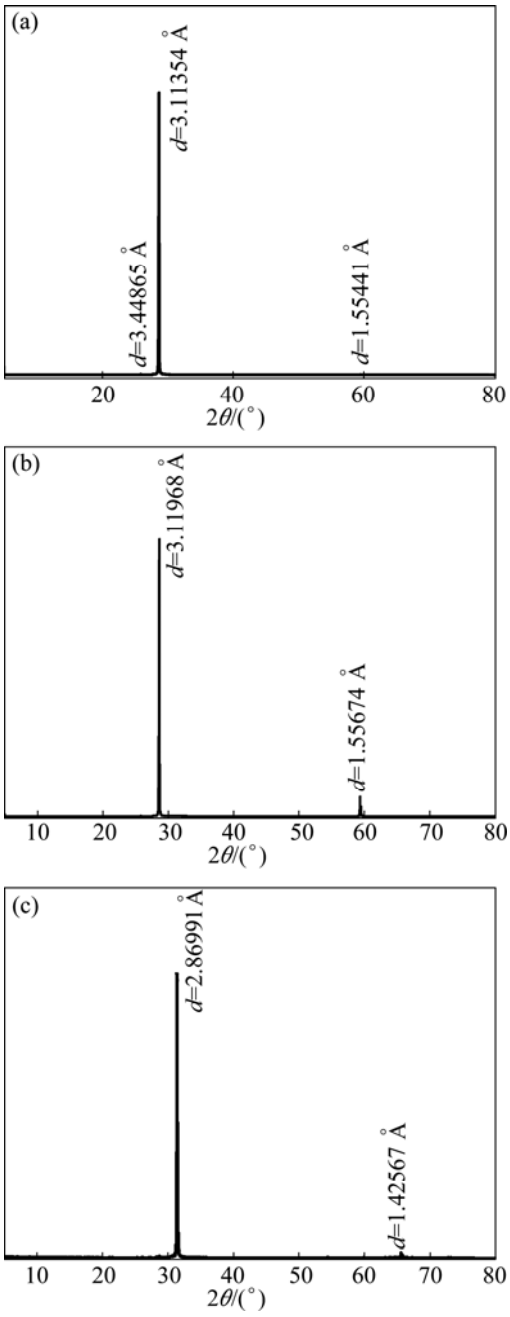

Fig. 2 XRD patterns of {112} cleavage surface (a), {112} crystal surface (b), {001} cleavage plane (c) of scheelite single crystal (*d*, interlayer spacing)

calculated interlayer spacing along {112} surfaces was 3.106 Å, which was larger than 2.844 Å along {001} surfaces, hence cleavage might generate more easily along {112} surfaces.

3.3 AFM study of three commonly exposed scheelite surfaces

Generally, the most commonly exposed mineral surfaces in the flotation slurry will be both cleavage planes and expressed crystal surfaces in the morphology of the mineral [3]. Surface topography and roughness may have an effect on surface reactivity towards the surrounding environment. The predominant {001} and {112} surfaces were chosen for the study of surface appearance of natural scheelite crystal by AFM.

As could be seen in Fig. 3(a), the {112} cleavage surface is rather flat and smooth, with a roughness (R_a) of only 0.532 nm, calculated using AFM software. In comparison, {112} crystal surface was rough, with a R_a of about 3.67 nm. On the surface, small hillocks with nonuniform sizes and shapes were observed, as shown in Fig. 3(b). On {001} cleavage surface, terraces were flat and separated by steps of about 10 nm in height, as shown in Fig. 3(c). The R_a of {001} surface was 7.08 nm

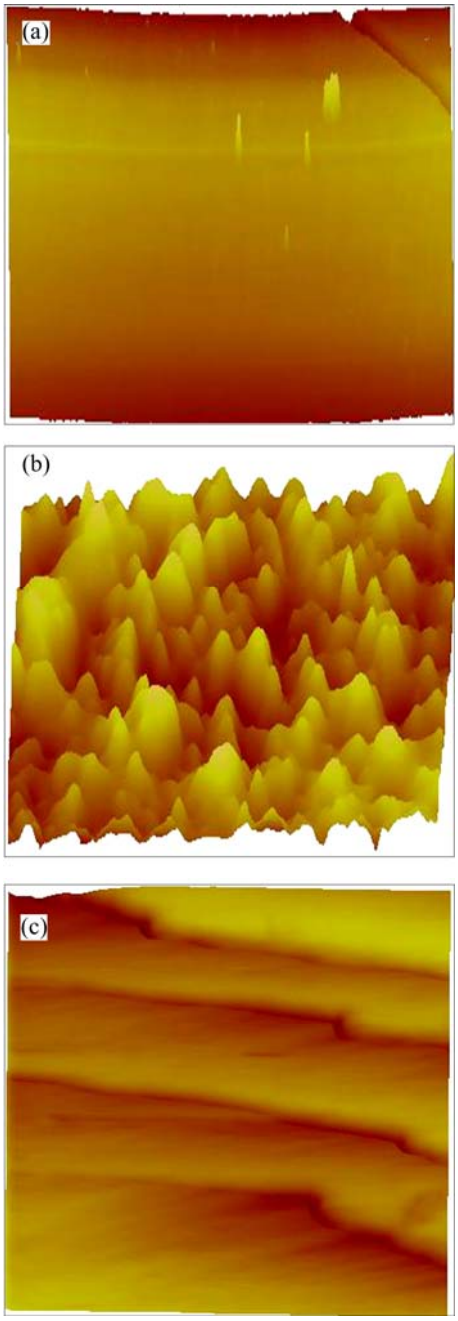

Fig. 3 AFM 3D images of {112} cleavage surface (a), {112} crystal surface (b) and {001} cleavage surface (c)

and the maximum protrusion was 71.5 nm. Compared with the stepped uneven {001} surface (Fig. 3(c)), the flat and smooth {112} surfaces (Fig. 3(a)) could experience cleavage more easily.

3.4 Wettability and surface energy measurement of three commonly exposed scheelite surfaces

Recent research showed that the contact angle and wetting behavior of crystalline solid surfaces were mainly influenced by surface roughness and heterogeneity [14,15]. As discussed in section 3.3, the roughness values of three commonly exposed surfaces were far below 0.1 μm. Such surfaces could generally be regarded as smooth ones in respect of contact angle measurements [16]. The contact angle measurement of several pure probe liquids with known surface tension parameters on a given solid surface was the common way of obtaining the surface energy of the solid material. In this study, the contact angles of three probe liquids on different scheelite surfaces are summarized in Table 2. Two of the liquids, i.e., water and formamide, were polar and diiodomethane was apolar one.

Table 2 Average contact angle measured by droplet on scheelite surface

Surface	Contact angle/(°)		
	Water	Formamide	Diiodomethane
{001} cleavage surface	73.1 (1.1)	57.1 (0.2)	30.1 (0.3)
{112} cleavage surface	62.7 (0.8)	41.4 (0.9)	22.8 (0.6)
{112} crystal surface	74.4 (3.1)	52.2 (0.7)	27.3 (0.7)

Note: The number in parentheses shows the standard deviation.

The static contact angle of water on {001} cleavage surface was larger than that on {112}. Since {112} cleavage surface had a larger surface dangling bond density and surface energy as discussed in section 3.2, it might demonstrate a more hydrophilic property and smaller contact angle than {001}. This difference in wettability could also be interpreted by the work of adhesion at scheelite surface−water interfaces. The work of adhesion (W_{sl}) between a solid surface and liquid could be described as [17]

$$W_{sl}=\gamma_l(1+\cos\theta) \quad (2)$$

where γ_l represents the liquid surface free energy; θ is the contact angle between the solid surface and the liquid. Accordingly, due to its larger surface dangling bond density and surface energy, the work of adhesion between {112} cleavage surface and water was 106.19 mJ/m^2, larger than 93.96 mJ/m^2 for {001}.

It is interesting to notice that the contact angle of water on {112} crystal surface is 74.4°, indicating a more hydrophobic property than on {112} cleavage surface. This might result from some apolar impurities present on {112} crystal surface and hence the relatively reduction of surface polar components, due to their prolonged exposure to the surrounding environment. Table 3 shows the surface energies and disperse and their polar components for different scheelite surfaces. The polar surface energy component of {112} crystal surface is smaller than that of freshly cleaved {112} surface. The work of adhesion between {112} crystal surface and water is 92.38 mJ/m^2, smaller than 106.19 mJ/m^2 for {112} cleavage surface.

Table 3 Surface energies with their disperse and polar components for different scheelite surfaces calculated according to methods after Owens−Wendt−Rabel−Kaeble

Surface	Surface energy/ (mJ·m^{-2})	Disperse component/ (mJ·m^{-2})	Polar component/ (mJ·m^{-2})
{001} cleavage surface	44.6	39.4	5.2
{112} cleavage surface	52	43.1	8.9
{112} crystal surface	46.5	42.1	4.4

In addition, the surface energy of {112} cleavage surface was higher than that of {001}, which was in agreement with the trend calculated using DFT. For all three surfaces, the polar components contributed less to their surface energies. This might be attributed to the fact that, in the creation of {001} and {112} surfaces, the coordination number of the calcium ions, which had eightfold coordination in the bulk material, was lowered to sixfold, as discussed in section 3.2. Six was a common coordination number for calcium (e.g. the solvated ion is coordinated to six water molecules) and hence the loss of bonding did not lead to enhanced reactivity of the surface calcium ions [2], resulting in a small polar component of surface energy.

4 Conclusions

1) The predominantly exposed surfaces in the morphologies of scheelite crystals were predicted by calculating surface energies using DFT. {112} and {001} cleavage surfaces and {112} crystal surface with the lowest surface energies were the commonly exposed surfaces, which were consistent with the previous literatures and the present experimental observations based on XRD. The cleavage generated more easily

along {112} surfaces than along {001} surfaces, which might be attributed to their different interlayer spacings.

2) The surface roughness and appearance of these commonly exposed surfaces were studied using AFM. The roughness of smooth {112} cleavage surface was the lowest among these three surfaces. On {001} cleavage surface, terraces were flat and separated by steps of about 10 nm in height. Compared with the surface appearances of {001} surfaces, the {112} surfaces could experience cleavage more easily.

3) The wettability and surface energies of the three surfaces were evaluated by contact angle measurements. The contact angle of water on {112} cleavage surface was less than that on {001} surface, due to a larger work of adhesion of {112} surface/water interface in comparison to {001} surface. The surface energies evaluated according to the contact angle measurement directly correspond to the trend calculated with DFT.

References

[1] PRADIP, RAI B, RAO T K, KRISHNAMURTHY S, VETRIVEL R, MIELCZARSKI J, CASES J M. Molecular modelling of interactions of diphosphonic acid based surfactants with calcium minerals [J]. Langmuir, 2002, 18(3): 932−940.

[2] COOPER T G, de LEEUW N H. A combined ab initio and atomistic simulation study of the surface and interfacial structures and energies of hydrated scheelite: Introducing a $CaWO_4$ potential model [J]. Surface Science, 2003, 531(2): 159−176.

[3] COOPER T G, de LEEUW N H. A computer modelling study of the competitive adsorption of water and organic surfactants at surfaces of the mineral scheelite [J]. Langmuir, 2004, 20(10): 3984−3994.

[4] MOGILEVSKY P. Identification of slip systems in $CaWO_4$ scheelite [J]. Philosophical Magazine, 2005, 85(30): 3511−3539.

[5] MOGILEVSKY P, PARTHASARATHY T A, PETRY M D. Anisotropy in room temperature microhardness and fracture of $CaWO_4$ scheelite [J]. Acta Materialia, 2004, 52(19): 5529−5537.

[6] GAO Zhi-yong, SUN Wei, HU Yue-hua, LIU Xiao-wen. Anisotropic surface broken bonds properties and wettability of calcite and fluorite crystals [J]. Transactions of Nonferrous Metals Society of China, 2012, 22(5): 1203−1208.

[7] ARYA A, CARTER E A. Structure, bonding, and adhesion at the ZrC interface from first principles [J]. Surface Science, 2004, 560(1−3): 103−120.

[8] PAYNE M C, TETER M P, ALLAN D C, ARIAS T A, JOANNOPOULOS J D. Iterative minimization techniques for ab initio total-energy calculations: Molecular dynamics and conjugate gradients [J]. Reviews of Modern Physics, 1992, 64(4): 1045−1097.

[9] PERDEW J P, BURKE K, ERNZERHOF M. Generalized gradient approximation made simple [J]. Physical Review Letters, 1996, 77(18): 3865−3868.

[10] KAY M I, FRAZER B C. ALMODOVAR I. Neutron diffraction refinement of $CaWO_4$ [J]. Journal of Chemical Physics, 1964, 40(2): 504−506.

[11] HAZEN R M, FINGER L W, MARIATHASAN J W E. High-pressure crystal chemistry of scheelite-type tungstates and molybdates [J]. Journal of Physics and Chemistry of Solids, 1985, 46(2): 253−263.

[12] HAY R S. TEM observations showing dislocations and twins in materials deformed at room temperature [J]. Ceramic Engineering and Science Proceedings, 2000, 21(4): 203−228.

[13] CHAUDHURI A R, PHANEUF L E. Grown-in dislocations in calcium tungstate crystals pulled from the melt [J]. Journal of Applied Physics, 1963, 34(8): 2162−2167.

[14] HENG J Y, BISMARCK A, LEE A F, WILSON K, WILLIAMS D R. Anisotropic surface energetics and wettability of macroscopic form I paracetamol crystals [J]. Langmuir, 2006, 22(6): 2760−2769.

[15] BUSSCHER H J, van PELT A W J, de BOER P, de JONG H P, ARENDS J. The effect of surface roughening of polymers on measured contact angles of liquids[J]. Colloids and Surfaces A: Physicochemical and Engineering, 1984, 9(4): 319−331.

[16] CHAU T T, BRUCKARD W J, KOH P T, NGUYEN A V. A review of factors that affect contact angle and implications for flotation practice [J]. Advances in Colloid and Interface Science, 2009, 150(2): 106−115.

[17] WANG S R, ZHANG Y, ABIDI N, CABRALES L. Wettability and surface free energy of graphene films [J]. Langmuir, 2009, 25(18): 11078−11081.

白钨矿晶体常见暴露面的表面能及表面形貌

高志勇，孙 伟，胡岳华，刘晓文

中南大学 资源加工与生物工程学院，长沙 410083

摘 要：采用密度泛函理论 DFT 计算白钨矿晶体 5 个晶面的表面能，预测白钨矿晶体常见的暴露面。预测分析表明，{112}和{001}解理面及{112}晶面是白钨矿晶体的 3 个主要暴露面，与文献报道的及 XRD 单晶衍射实验结果一致。较{001}面方向，沿{112}面层间更容易产生解理，可能与这两个晶面方向的层间距差异有关。采用 AFM 研究 3 个常见暴露面的表面形貌。研究表明，{112}解理面最光滑，粗糙度最小；在{001}解理面上高度约 10 nm 的台阶依次排列。采用接触角测量的方法研究 3 个暴露面的润湿性，并计算其表面能。计算所得的表面能数据与 DFT 计算值大小顺序一致。

关键词：白钨矿；表面能；解理；接触角；润湿性

(Edited by Xiang-qun LI)